Inorganic Chemistry

pubs.acs.org/IC

Communication

Robust 4d−5f Bimetal−Organic Framework for Efficient Removal of Trace SO_2 from SO_2/CO_2 and $SO_2/CO_2/N_2$ Mixtures

Li Juan Guo, Xue Feng Feng, Zhi Gao, Rajamani Krishna, and Feng Luo*

Cite This: *Inorg. Chem.* 2021, 60, 1310−1314

Read Online

ACCESS | Metrics & More | Article Recommendations | Supporting Information

ABSTRACT: Herein, we report a highly rare robust 4d−5f bimetal−organic framework that shows high porosity and thermal/chemical stability and thus is capable of removing trace SO_2 from a $SO_2/CO_2/N_2$ mixture even under humid conditions. This work not only shows a novel adsorbent for SO_2 removal but also extends the function of actinium-based coordination compounds.

The treatment of air pollutants is the main link of contemporary environmental protection.[1,2] As the main body of urban pollutants, sulfur dioxide (SO_2) is mainly produced in the combustion of sulfur-containing fuels, smelting of a sulfur-containing ore, sulfuric acid production, and petroleum refining. The traditional technology for treating SO_2 is flue-gas desulfurization (FGD). However, this process produces a lot of sewage, and more seriously 2000 ppm of SO_2 still remains.[3,4] Therefore, the search for efficient and environmentally friendly SO_2 flue-gas-treatment technology has aroused great interest for researchers.

Metal−organic frameworks (MOFs) present a new type of porous material[5−7] often showing regular pores, a high specific surface, a functionalized pore wall by the organic unit, and sometimes an open-metal site, opening them to broad applications in gas storage and separation, sensing, catalysis, and so on.[8,9] For separation scopes, in contrast to separations such as C_2H_2/CO_2, C_2H_4/C_2H_6, C_2H_4/C_2H_2, and Xe/Kr,[10−14] there are relatively few reports on the application of MOFs for the separation of SO_2, mainly because of the strong acidity and causticity of SO_2 molecules, which could seriously destroy the MOF adsorbent during the separation process. Thereby, MOFs available for the removal of SO_2, especially under humid conditions, have been extremely scarce until now. Recently, using MOFs for SO_2 removal has received increasing attention. For example, MOF-177[15] revealed a new record high SO_2 uptake (25.7 mmol/g at 293 K and 1 bar). Schröder et al.[16] reported a high SO_2 adsorption capacity of 12.3 mmol/g at 298 K and 1.0 bar. SO_2 adsorption in MFM-601 is fully reversible and highly selective over CO_2 and N_2. Mon et al.[17] reported a new type of 3D MOF, where the weak supramolecular interaction between SO_2 and coordinated water molecules triggers the selective and reversible SO_2 adsorption. Zhang et al.[18] disclosed a dual specific adsorption site for SO_2 in CPL-1 by dispersion-corrected density functional theory. Xing et al.[19] created record SO_2/CO_2 selectivity in SIFSIX-2-Cu-i. Ibarra et al.[20] observed an effective approach to enhancing the SO_2 adsorption capacity by loading a small amount of C_2H_5OH into the adsorbent. Although SO_2 removal has been successfully achieved by MOFs, weaknesses such as the stability of MOFs, SO_2 selectivity, and separation ability under humid conditions still need to be overcome.

In this work, we report a new MOF for SO_2 removal, especially under humid conditions. Also, in the following sections, the synthesis, structure, and SO_2 removal are discussed in detail.

The MOF **ECUT-100** [$(UO_2)Cd(L)_2$, where H_2L = 2,4-pyridinedicarboxylic acid] was synthesized by a mixture of $Cd(NO_3)_2{\cdot}4H_2O$ (0.049 mmol, 15 mg), $UO_2(NO_3)_2{\cdot}6H_2O$ (0.03 mmol, 16.7 mg), and H_2L (0.1 mmol, 16.7 mg) in a mixed solution of *N*,*N*-dimethylformamide (DMF; 4 mL) and C_2H_6OH (1 mL) with 200 μL of $HClO_4$. The reaction temperature and time were 120 °C and 3 days. Pure yellow block crystals were obtained with yields of up to 90% based on Cd. The phase purity was confirmed by powder X-ray diffraction (PXRD; Figure S1).

The structure was determined by single-crystal X-ray diffraction, giving a monoclinic crystal system and *C*2/*c* space group. The symmetric unit contains one Cd center, one U center, and two L^{2-} ligands. Cd1 is coordinated by four L^{2-} O atoms and two L^{2-} N atoms, creating a somewhat distorted octahedral configuration (Figure 1a). The U1 site is a typical uranyl ion, showing the U≡O bond (O4 and O5) on the orbital plane with a bond length of 1.77 (2) Å, located in the normal range, while O1, O2, O3, O6, O7, and O8 from the L^{2-} ligands locate on the equatorial plane, resulting in the overall pentagonal-bipyramidal configuration for the U1 site (Figure 1a). The Cd−O/N and U−O bond lengths are in the normal range. The L^{2-} ligands use both the carboxylate and pyridine N atoms to bind with metal ions, rendering two distinct coordination modes for carboxylate groups, one showing the dibidentate mode for the two carboxylate groups and the other

Received: December 2, 2020
Published: January 15, 2021

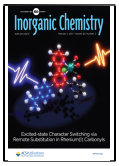

https://dx.doi.org/10.1021/acs.inorgchem.0c03526
Inorg. Chem. 2021, 60, 1310−1314

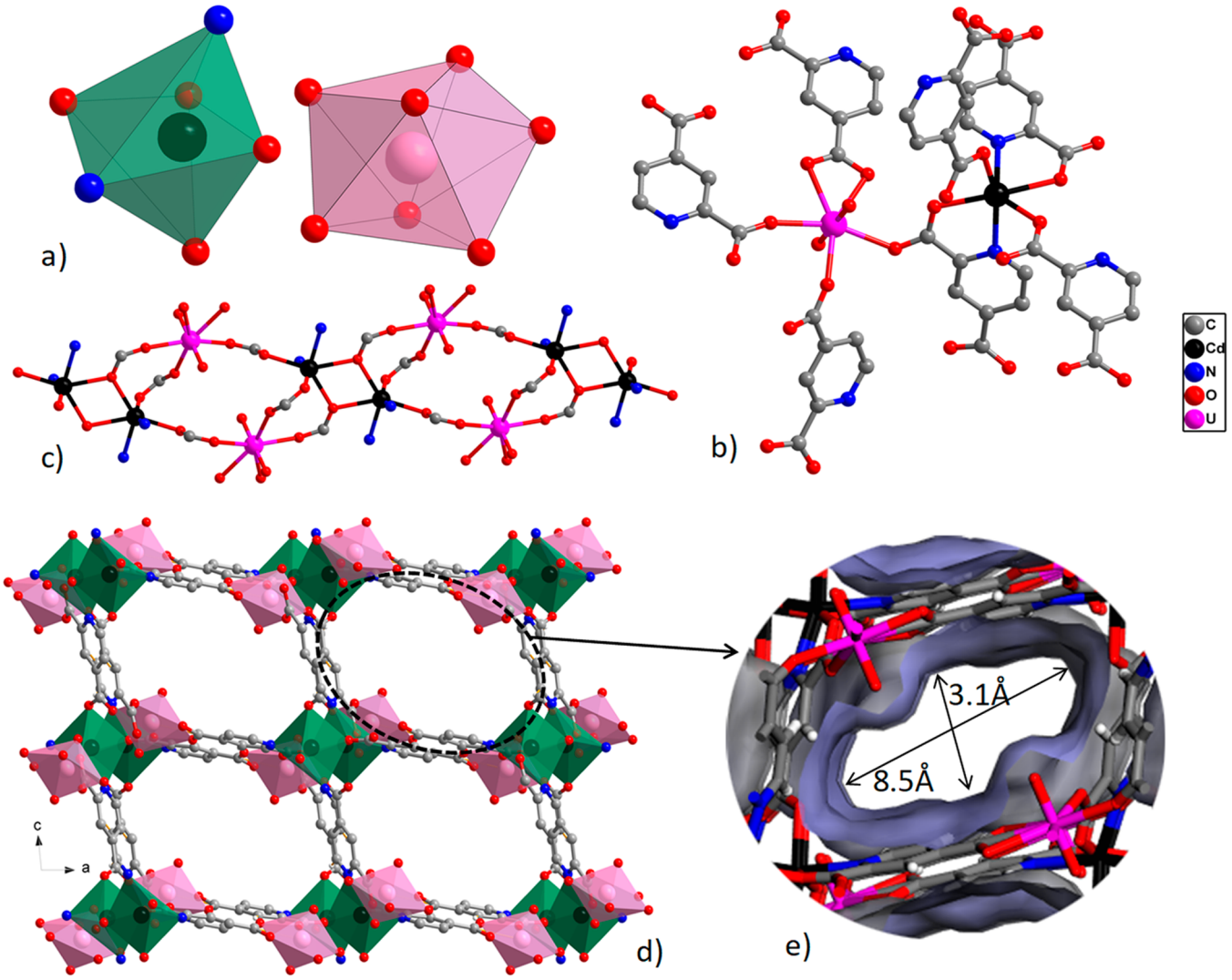

Figure 1. (a) Coordination polyhedra of Cd and U atoms. (b) Coordination surrounding the metal ions. (c) Rod-shaped secondary building unit constructed by in turn connected 4- and 16-membered rings. (d) 3D framework with the 1D channel. (e) Connolly surface of the 1D channel.

one showing chelate *plus* tridentate mode for the two carboxylate groups (Figure 1a,b) .

For **ECUT-100**, a structural feature is a unique rod secondary building block. As shown in Figure 1c, along the *b* axis, two Cd^{II} ions are combined together by two carboxylate O atoms (O10) to give a 4-membered-ring dinuclear fragment (Figure 1b), which further connects to four U^{VI} ions through four carboxyl groups, resulting in the 16-membered-ring tetranuclear fragment. Interestingly, these 4- and 16-membered rings are in turn connected together to construct the overall rod secondary building block (Figure 1c). Each rod connects to four identical rods, generating the final rod packing framework (Figure 1d). Along the *b* axis, a clear 1D rectangle-like channel is observed. However, because of the location of the U≡O bond within the pore, a narrow but long pore with a size of 3.1 Å × 8.5 Å was thus observed in **ECUT-100** (Figure 1e). The solvent-accessible volume estimated by *Platon*[21] is 43.3% of the cell volume (Figure 1e), occupied by disordered solvent molecules.

To test the stability of **ECUT-100**, thermogravimetric analysis was initially performed (Figure S2). Two major losses at 30−84 and 130−340 °C belong to the loss of one C_2H_5OH molecule (exptl 5.5%; calcd 5.4%) and 1.5 DMF molecules (exptl 11.6%; calcd 12.4%). Thus, the chemical formula of **ECUT-100** is $(UO_2)Cd(L)_2{\cdot}(C_2H_5OH)(DMF)_{1.5}$. Then we tested the CH_3OH-exchanged samples, where the loss of solvent molecules is at 30−140 °C, meaning that DMF molecules were completely exchanged by CH_3OH. Accordingly, the activating temperature was set as 140 °C.

The permanent porosity was confirmed by N_2 adsorption at 77 K. A typical type I adsorption was observed, suggesting a microporous framework of **ECUT-100**. The Brunauer−Emmett−Teller specific surface area was calculated to be 688 m^2/g (Figure 2a) with a total pore volume of 0.27 cm^3/g. A narrow pore distribution among 5.5 Å was observed, comparable with the crystal data.

We further carried out SO_2 adsorption tests (Figures 2b and S3). Interestingly, a step adsorption of SO_2 in the low-pressure range was observed, indicating a high affinity of the framework toward SO_2. For any separation, the step adsorption isotherm in the low-pressure range is highly desirable, which implies high selectivity. Especially for SO_2 removal, the magnitude of SO_2 uptake at low pressure is highly important because almost all SO_2-containing products just contain a trace amount of SO_2 in the level of parts per million. Then we analyze the adsorption data at low pressure. At 0.01 bar and 298 K, the

https://dx.doi.org/10.1021/acs.inorgchem.0c03526
Inorg. Chem. 2021, 60, 1310−1314

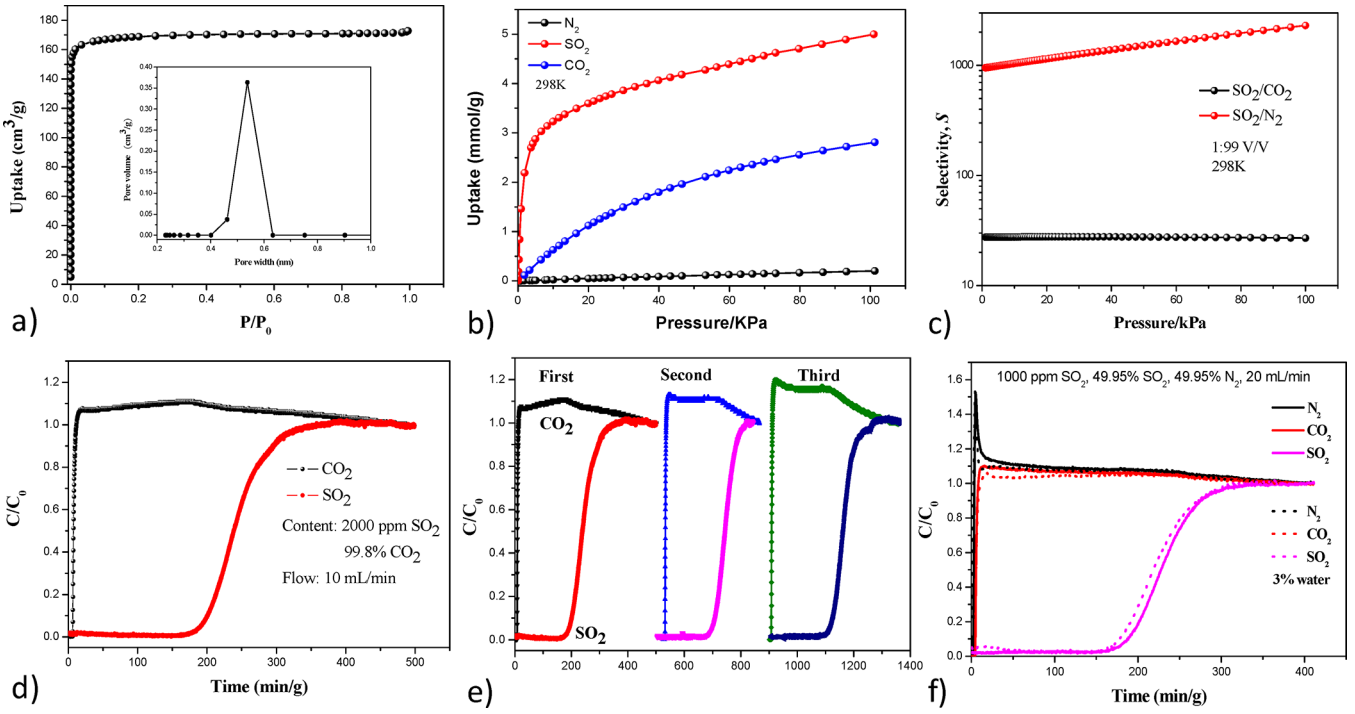

Figure 2. (a) N_2 adsorption isotherm at 77 K and pore distribution. (b) CO_2, SO_2, and N_2 adsorption isotherms at 298 K (highlighted is the low-pressure section). (c) SO_2 adsorption selectivity over CO_2 and N_2 for a 1:99 (v/v) SO_2/CO_2 or SO_2/N_2 mixture. (d) Breakthrough experiments based on a **ECUT-100** bed (1.5 g) under a 10 mL/min flow for a SO_2/CO_2 mixture containing 2000 ppm of SO_2. (e) Recycle use of a **ECUT-100** bed for the separation of a SO_2/CO_2 mixture. (f) Comparison of the separations of a $SO_2/CO_2/N_2$ mixture without water and with 3% water.

SO_2 uptake is as high as 1.88 mmol/g, comparable with those of some top-performing MOFs such as SIFSIX-3-Zn (1.68 mmol/g)[19] and SIFSIX-3-Ni (2.43 mmol/g).[19] At 0.1 bar, the SO_2 uptake increases to 3.3 mmol/g, bigger than those of some top-performing MOFs such as SIFSIX-3-Zn (1.89 mmol/g),[19] SIFSIX-3-Ni (2.55 mmol/g),[19] and MFM-202a (3.0 mmol/g).[22] At 1 bar, the adsorption capacity is 4.95 mmol/g, bigger than those of commercial porous carbon (3.3 mmol/g) and some MOFs such as SIFSIX-3-Zn (2.1 mmol/g),[19] SIFSIX-3-Ni (2.74 mmol/g),[19] P(TMGA-*co*-MBA) (4.06 mmol/g),[23] and MOF-74 (3.03 mmol/g).[24] By contrast, the CO_2 adsorptions at 1, 0.1, and 0.01 bar are 2.76, 0.71, and 0.08 mmol/g, suggesting the highly selective adsorption of SO_2 over CO_2 at low pressure.

Because of the trace amount of SO_2 in the SO_2-containing product, we first estimated the Henry constant and selectivity based on the adsorption data at low pressure (Figure S4). The Xe Henry constant is 177 (mmol/g)/bar, whereas the corresponding value for CO_2 is 6 (mmol/g)/bar (Figure S5), resulting in high Henry selectivities of up to 29.5. Moreover, on the basis of ideal adsorbed solution theory (IAST) calculations (Figure 2c), we can obtain theoretical SO_2/CO_2 selectivities among all adsorption processes, giving selectivities of 27.5−26.9 for a 1:99 (v/v) SO_2/CO_2 mixture, comparable with the Henry selectivity. The value is also close to that of one of the benchmark MOFs, MFM-170 (S = 28).[25]

To obtain the SO_2/CO_2 separation ability on **ECUT-100**, we carried out both simulated breakthrough calculation and dynamic breakthrough experiments, confirming its big potential in the removal of SO_2 from a SO_2/CO_2 mixture with 2000 ppm of SO_2. Breakthrough calculation for a 1:99 (v/v) SO_2/CO_2 mixture discloses complete separation with a separation time of $\Delta\tau$ = 3500 (Figure S6). Dynamic breakthrough experiments on the **ECUT-10** column also render complete separation for a SO_2/CO_2 mixture containing 2000 ppm of SO_2, where CO_2 breaks the column within 6 min/g, but the retention time for SO_2 is as long as 160 min/g, confirming its real SO_2 separation ability for a simulated flue gas (Figure 2d). Impressively, repeating this dynamic breakthrough experiment three times does not reduce its separation performance, suggesting its excellent recycle use, an important factor for its practical application (Figure 2e).

As we know, flue gas also contains a great deal of N_2, except for CO_2 and SO_2. Then, we next tested the N_2 adsorption at 298 K (Figure 2b). The N_2 uptakes at 1, 0.1, and 0.01 bar are 0.2, 0.025, and 0.0035 mmol/g, implying the ultrahighly selective adsorption of SO_2 over N_2. The corresponding Henry constant, Henry selectivity, and IAST selectivity are 0.2 (mmol/g)/bar, 895, and 950−2302 (Figure S7, 2c). The value of the IAST selectivity is comparable with that observed in SIFSIX-1-Cu (S = 2510)[19] and larger than those in SIFSIX-2-Cu-I (S = 1285)[19] and MFM-170 (S = 260).[25] Furthermore, similar simulated breakthrough calculation and dynamic breakthrough experiments were carried out. We carried out breakthrough experiments for a $SO_2/CO_2/N_2$ mixture containing 1000 ppm of SO_2. The separation time of $\Delta\tau$ = 7540 for SO_2 from a $SO_2/CO_2/N_2$ mixture was estimated from simulated breakthrough calculation, suggesting complete separation (Figure S8). The dynamic breakthrough experiments of a $SO_2/CO_2/N_2$ mixture are shown in Figure 2f, where N_2 immediately breaks the column within 1 min/g, then CO_2 follows within 5 min/g, and after 151 min/g outflow of SO_2 is detected. These breakthrough experiments were further executed three times without any decrease in the performance, implying excellent recycle use (Figure S9). In addition, we also found that moisture (3% water) has little effect on the

https://dx.doi.org/10.1021/acs.inorgchem.0c03526
Inorg. Chem. 2021, 60, 1310−1314

separation performance (Figure 2f), indicative of its superior application for real flue gas. The stability after breakthrough experiments was also confirmed by PXRD (Figure S1) and a photograph of **ECUT-100** (Figure S10).

In conclusion, a novel Cd−U MOF of **ECUT-100** was constructed by a bimetal approach. This MOF contains a highly rare rod-shaped secondary building unit composed of in turn connected 4- and 16-membered rings, thus affording high thermal and chemical stability. The high porosity and matchable pore size for SO_2 over CO_2 lead to both high SO_2 uptake and selectivity at low pressure, finally resulting in the complete separation of SO_2 from a SO_2/CO_2 or $SO_2/CO_2/N_2$ mixture with a parts-per-million-level SO_2. Most importantly, this separation can also be highly effective under moisture conditions, fully meeting the practical application of FGD. For SO_2 removal such as FGD, it owns a complicated system; thus, further investigation close to the real environment is needed. Moreover, the cost of MOFs is also an important factor.

■ ASSOCIATED CONTENT

Supporting Information

The Supporting Information is available free of charge at https://pubs.acs.org/doi/10.1021/acs.inorgchem.0c03526.

Materials including the synthesis in detail and additional figures (PDF)

Accession Codes

CCDC 2047397 contains the supplementary crystallographic data for this paper. These data can be obtained free of charge via www.ccdc.cam.ac.uk/data_request/cif, or by emailing data_request@ccdc.cam.ac.uk, or by contacting The Cambridge Crystallographic Data Centre, 12 Union Road, Cambridge CB2 1EZ, UK; fax: +44 1223 336033.

■ AUTHOR INFORMATION

Corresponding Author

Feng Luo − *School of Biology, Chemistry and Material Science, East China University of Technology, Nanchang, Jiangxi 344000, China;* orcid.org/0000-0001-6380-2754; Email: ecitluofeng@163.com

Authors

Li Juan Guo − *School of Biology, Chemistry and Material Science, East China University of Technology, Nanchang, Jiangxi 344000, China*

Xue Feng Feng − *School of Biology, Chemistry and Material Science, East China University of Technology, Nanchang, Jiangxi 344000, China*

Zhi Gao − *School of Biology, Chemistry and Material Science, East China University of Technology, Nanchang, Jiangxi 344000, China*

Rajamani Krishna − *Van't Hoff Institute for Molecular Sciences, University of Amsterdam, 1098 XH Amsterdam, The Netherlands;* orcid.org/0000-0002-4784-8530

Complete contact information is available at: https://pubs.acs.org/10.1021/acs.inorgchem.0c03526

Author Contributions

The manuscript was written through contributions of all authors.

Notes

The authors declare no competing financial interest.

■ ACKNOWLEDGMENTS

We thank the National Science Foundations of China (Grants 21966002, 21871047, and 21761001), the Natural Science Foundation of Jiangxi Province of China (Grant 20181ACB20003), and the Training Program for Academic and Technical Leaders of Major Disciplines in Jiangxi Province (Grant 20194BCJ22010).

■ REFERENCES

(1) Belmabkhout, Y.; Bhatt, P. M.; Adil, K.; Pillai, R. S.; Cadiau, A.; Shkurenko, A.; Maurin, G.; Liu, G.; Koros, W. J.; Eddaoudi, M. Natural gas upgrading using a fluorinated MOF with tuned H_2S and CO_2 adsorption selectivity. *Nat. Energy.* **2018**, *3*, 1059−1066.

(2) Laurent, A.; Espinosa, N. Environmental impacts of electricity generation at global, regional and national scales in 1980−2011: what can we learn for future energy planning? *Energy Environ. Sci.* **2015**, *8*, 689−701.

(3) Fioletov, V. E.; McLinden, C. A.; Krotkov, N.; Li, C.; Joiner, J.; Theys, N.; Carn, S.; Moran, M. D. A global catalogue of large SO_2 sources and emissions derived from the ozone monitoring instrument. *Atmos. Chem. Phys.* **2016**, *16*, 11497−11519.

(4) Yuan, J.; Jiang, X.; Chen, D.; Jiang, W.; Li, J. Evolution of sulfur species on titanium ore modified activated coke during flue gas desulfurization. *Energy Fuels* **2018**, *32*, 8623−8630.

(5) Zhu, L.; Liu, X. Q.; Jiang, H. L.; Sun, L. B. Metal-organic frameworks for heterogeneous basic catalysis. *Chem. Rev.* **2017**, *117*, 8129−8176.

(6) Yang, Q. H.; Xu, Q.; Jiang, H. L. Metal-organic frameworks meet metal nanoparticles: synergistic effect for enhanced catalysis. *Chem. Soc. Rev.* **2017**, *46*, 4774−4808.

(7) Cohen, S. M. Postsynthetic methods for the functionalization of metal-organic frameworks. *Chem. Rev.* **2012**, *112*, 970−1000.

(8) Carter, J. H.; Han, X.; Moreau, F. Y.; Da Silva, I.; Nevin, A.; Godfrey, H. G. W.; Tang, C. C.; Yang, S.; Schröder, M. Exceptional adsorption and binding of sulfur dioxide in a robust zirconium based metal-organic framework. *J. Am. Chem. Soc.* **2018**, *140*, 15564−15567.

(9) Stock, N.; Biswas, S. Synthesis of metal-organic frameworks (MOFs):routes to various of topologies, morphologies, and composites. *Chem. Rev.* **2012**, *112*, 933−969.

(10) (a) Li, B.; Wen, H. M.; Zhou, W.; Xu, J. Q.; Chen, B. L. Porous metal-organic frameworks: promising materials for methane storage. *Chem.* **2016**, *1*, 557−580. (b) Zhang, H. P.; Fan, Y. L.; Krishna, R.; Feng, X. F.; Wang, L.; Luo, F. Robust metal-organic framework with multiple traps for trace Xe/Kr separation. *Sci. Bull.* **2020**, DOI: 10.1016/j.scib.2020.12.031. (c) Fan, Y. L.; Zhang, H. P.; Yin, M. J.; Krishna, R.; Feng, X. F.; Wang, L.; Luo, M. B.; Luo, F. High adsorption capacity and selectivity of SO_2 over CO_2 in a metal-organic framework. *Inorg. Chem.* **2021**, *60*, 4.

(11) Cui, X. L.; Chen, K. J.; Xing, H. B.; Yang, Q. W.; Krishna, R.; Bao, Z. B.; Wu, H.; Zhou, W.; Dong, X. L.; Han, Y.; Li, B.; Ren, Q. L.; Zaworotko, M. J.; Chen, B. L. Pore chemistry and size control in hybrid porous materials for acetylene capture from ethylene. *Science* **2016**, *353*, 141−144.

(12) Shi, Z. L.; Tao, Y.; Wu, J. S.; Zhang, C. Z.; He, H. L.; Long, L. L.; Lee, Y. J.; Li, T.; Zhang, Y. B. Robust metal-triazolate frameworks for CO_2 capture from flue gas. *J. Am. Chem. Soc.* **2020**, *142*, 2750−2754.

(13) Peng, Y. L.; Pham, T.; Li, P. F.; Wang, T.; Chen, Y.; Chen, K. J.; Forrest, K. A.; Space, B.; Cheng, P.; Zaworotko, M. J.; Zhang, Z. J. Robust ultramicroporous metal-organic frameworks with benchmark affinity for acetylene. *Angew. Chem., Int. Ed.* **2018**, *57*, 10971−10975.

(14) (a) Luo, F.; Yan, C. S.; Dang, L. L.; Krishna, R.; Zhou, W.; Wu, H.; Dong, X. L.; Han, Y.; Hu, T. L.; O'Keeffe, M.; Wang, L. L.; Luo, M. B.; Lin, R. B.; Chen, B. L. UTSA-74: a MOF-74 isomer with two accessible binding sites per metal center for highly selective gas separation. *J. Am. Chem. Soc.* **2016**, *138*, 5678−5684. (b) Xu, Z. Z.; Xiong, X. H.; Xiong, J. B.; Krishna, R.; Li, L. B.; Fan, Y. L.; Luo, F.; Chen, B. L. A robust Th-azole framework for highly efficient

purification of C_2H_4 from a $C_2H_4/C_2H_2/C_2H_6$ mixture. *Nat. Commun.* **2020**, *11*, 3163. (c) Tao, Y.; Fan, Y. L.; Xu, Z. Z.; Feng, X. F.; Krishna, R.; Luo, F. Boosting selective adsorption of Xe over Kr by double-accessible open-metal site in metal-organic framework: experimental and theoretical research. *Inorg. Chem.* **2020**, *59*, 11793−11800. (d) Fu, X. P.; Wang, Y. L.; Liu, Q. Y. Metal-organic frameworks for C_2H_2/CO_2 separation. *Dalton Trans* **2020**, *49*, 16598−16607. (f) Liu, R.; Liu, Q. Y.; Krishna, R.; Wang, W. J.; He, C. T.; Wang, Y. L. Water-stable europium 1,3,6,8-tetrakis (4-carboxylphenyl)pyrene framework for efficient C_2H_2/CO_2 separation. *Inorg. Chem.* **2019**, *58*, 5089−5095.

(15) Brandt, P.; Nuhnen, A.; Lange, M.; Möllmer, J.; Weingart, O.; Janiak, C. Metal-organic frameworks with potential application for SO_2 separation and flue gas desulfurization. *ACS Appl. Mater. Interfaces* **2019**, *11*, 17350−17358.

(16) Carter, J. H.; Han, X.; Moreau, F. Y.; da Silva, I.; Nevin, A.; Godfrey, H. G. W.; Tang, C. C.; Yang, S. H.; Schröder, M. Exceptional adsorption and binding of sulfur dioxide in a robust zirconium-based metal-organic framework. *J. Am. Chem. Soc.* **2018**, *140*, 15564−15567.

(17) Mon, M.; Tiburcio, E.; Ferrando-Soria, J.; Gil San Millán, R.; Navarro, J. A. R.; Armentano, D.; Pardo, E. A post-synthetic approach triggers selective and reversible sulphur dioxide adsorption on a metal-organic framework. *Chem. Commun.* **2018**, *54*, 9063−9066.

(18) Zhang, Y.; Chen, Z. H.; Liu, X.; Dong, Z.; Zhang, P. X.; Wang, J.; Deng, Q.; Zeng, Z. L.; Zhang, S. H.; Deng, S. G. Efficient SO_2 removal using a microporous metal-organic framework with molecular sieving effect. *Ind. Eng. Chem. Res.* **2020**, *59*, 874−882.

(19) Cui, X.; Yang, Q. W.; Yang, L. F.; Krishna, R.; Zhang, Z. G.; Bao, Z. B.; Wu, H.; Ren, Q. L.; Zhou, W.; Chen, B. L.; Xing, H. B. Ultrahigh and selective SO_2 uptake in inorganic anion-pillared hybrid porous materials. *Adv. Mater.* **2017**, *29*, 1606929.

(20) Zárate, J. A.; Sánchez-González, E.; Williams, D. R.; González-Zamora, E.; Martis, V.; Martínez, A.; Balmaseda, J.; Maurin, G.; Ibarra, I. A. High and energy-efficient reversible SO_2 uptake by a robust Sc(III)-based MOF. *J. Mater. Chem. A* **2019**, *7*, 15580−15584.

(21) Blatov, V. A.; Shevchenko, A. P. *TOPOS 4.0*; Samara State University: Samara Oblast, Russia, 1999.

(22) Yang, S. H.; Liu, L. F.; Sun, J. L.; Thomas, K. M.; Davies, A. J.; George, M. W.; Blake, A. J.; Hill, A. H.; Fitch, A. N.; Tang, C. C.; Schröder, M. Irreversible network transformation in a dynamic porous host catalyzed by sulfur dioxide. *J. Am. Chem. Soc.* **2013**, *135*, 4954−4957.

(23) Wu, L. B.; An, D.; Dong, J.; Zhang, Z. M.; Li, B. G.; Zhu, S. P. Preparation and SO_2 absorption/desorption properties of crosslinked poly(1,1,3,3-tetramethylguanidine acrylate) porous particles. *Macromol. Rapid Commun.* **2006**, *27*, 1949−1954.

(24) Britt, D.; Tranchemontagne, D.; Yaghi, O. M. Metal-organic frameworks with high capacity and selectivity for harmful gases. *Proc. Natl. Acad. Sci. U. S. A.* **2008**, *105*, 11623−11627.

(25) Smith, G. L.; Eyley, J. E.; Han, X.; Zhang, X. R.; Li, J. N.; Jacques, N. M.; Godfrey, H. G. W.; Argent, S. P.; McCormick McPherson, L. J.; Teat, S. J.; Cheng, Y. Q.; Frogley, M. D.; Cinque, G.; Day, S. J.; Tang, C. C.; Easun, T. L.; Rudić, S.; Ramirez-Cuesta, A. J.; Yang, S. H.; Schröder, M. Reversible coordinative binding and separation of sulfur dioxide in a robust metal-organic framework with open copper sites. *Nat. Mater.* **2019**, *18*, 1358−1365.

https://dx.doi.org/10.1021/acs.inorgchem.0c03526
Inorg. Chem. 2021, 60, 1310−1314

A Robust 4d-5f Bimetal-Organic Framework for Efficient Removal of Trace SO_2 from SO_2/CO_2 and $SO_2/CO_2/N_2$ Mixture

Li Juan Guo,[a] Xue Feng Feng,[a] Zhi Gao, [a] Rajamani Krishna,[b] and Feng Luo [a]*

[a]School of Biology, Chemistry and Material Science, East China University of Technology, Nanchang, Jiangxi 344000, China

[b]Van't Hoff Institute for Molecular Sciences, University of Amsterdam, Science Park 904, 1098 XH Amsterdam, The Netherlands

Experimental Methods

Materials and Physical Measurements. All chemicals are directly purchased from innochem with no further purification. The data of X-ray powder diffraction were collected on a Bruker AXSD8 Discover powder diffractometer at 40 kV/40 mA for Cu Kα (λ = 1.5406 Å) at room temperature in the range of 5-50 °(2θ) with a scan speed of 0.1 °per step. Thermogravimetric analysis (TG) was performed by a TGA Q500 thermal analysis system. All TGA experiments were performed under a N_2 atmosphere from 40-800°C at a rate of 5°C /min. The gas sorption isotherms were collected on ASAP2020 PLUS (anti-corrosion version). Ultrahigh-purity-grade (>99.999%) N_2, CO_2, and SO_2 gases were used in this adsorption measurement. To maintain the experimental temperatures liquid nitrogen (77 K) and temperature-programmed water bath (273 and 298 K) were used respectively.

Synthesis of ECUT-100. 2,4- pyridinedicarboxylic acid (0.1 mmol, 16.7 mg)， $Cd(NO_3)_2 \cdot 4H_2O$ (0.049 mmol, 15 mg) and $UO_2(NO_3)_2 \cdot 6H_2O$ (0.03 mmol, 16.7 mg) in a mixed solution of DMF (4mL) and C_2H_6OH (1mL) with 200 μL $HClO_4$. The reaction temperature and time is 120℃ and three day. Pure yellow block crystals were obtained with yield up to 90% based on Cd. The element analysis (%) is, calc. C/20.31, H/1.87, N/2.31; exp. C/20.40, H/1.85, N/2.39.

Caution! U used in this study is an α emitter. All U compounds used and investigated were operated in an authorized laboratory designed for actinide element studies. Standard precautions for handling radioactive materials should be followed.

Degassing ECUT-100. 100 mg MOF crystals were soaked in methanol for three days and fresh methanol was added every 8 h. After decanting the methanol extract, the sample was dried at room temperature overnight, then further degassed using ASAP2020 PLUS for 24 h at 140°C.

X-ray Crystallography. X-ray diffraction data of **ECUT-100** were collected at room temperature on a Bruker Appex II CCD diffractometer using graphite monochromated MoKα radiation (λ=0.71073 Å). The data reduction included a correction for Lorentz and polarization effects, with an applied multi-scan absorption correction (SADABS). The crystal structure was solved and refined using the SHELXTL program suite. Direct methods yielded all non-hydrogen atoms, which were refined with anisotropic thermal parameters. All hydrogen atom positions were calculated geometrically and were riding on their respective atoms. The SQUEEZE subroutine of the PLATON software suite was used to remove the scattering from the highly disordered guest molecules. CCDC 2047397 contains the supplementary crystallographic data of **ECUT-100**. These data can be obtained free of charge from the Cambridge Crystallographic Data Centre via www.ccdc.cam.ac.uk/data_request/cif.

Isosteric heat of adsorption

The binding energy is reflected in the isosteric heat of adsorption, Q_{st}, is calculated from the Clausius-Clapeyron equation

$$Q_{st} = -RT^2 \left(\frac{\partial \ln p}{\partial T} \right)_q \quad \square\square\square\ \square$$

For the1-site Langmuir-Freundlich model the differentiation of the Clausius Clapeyron equation can be carried out analytically.

IAST calculations of adsorption selectivities and uptake capacities

We consider the separation of binary 1/99 SO_2/CO_2 mixtures and 1/99 SO_2/N_2 mixtures at 298 K. The adsorption selectivity for SO_2/CO_2 and SO_2/N_2 separation is defined by

$$S_{ads} = \frac{q_1/q_2}{p_1/p_2}$$

Transient breakthrough simulations

The performance of industrial fixed bed adsorbers is dictated by a combination of adsorption selectivity and uptake capacity. Transient breakthrough simulations were carried out using the methodology described in earlier publications. The following two mixtures were investigated.

1/99 SO_2/CO_2 mixtures at 298 K and 100 kPa,

1/49.5/49.5 $SO_2/CO_2/N_2$ mixtures at 298 K and 100 kPa,

For the breakthrough simulations, the following parameter values were used: length of packed bed, L = 0.3 m; voidage of packed bed, ε = 0.4; superficial gas velocity at inlet, u = 0.04 m/s.

The *y*-axis is the dimensionless concentrations of each component at the exit of the fixed bed, c_i/c_{i0} normalized with respect to the inlet feed concentrations. The *x*-axis is the *dimensionless* time, $\tau = \frac{tu}{L\varepsilon}$, defined by dividing the actual time, *t*, by the characteristic time, $\frac{L\varepsilon}{u}$.

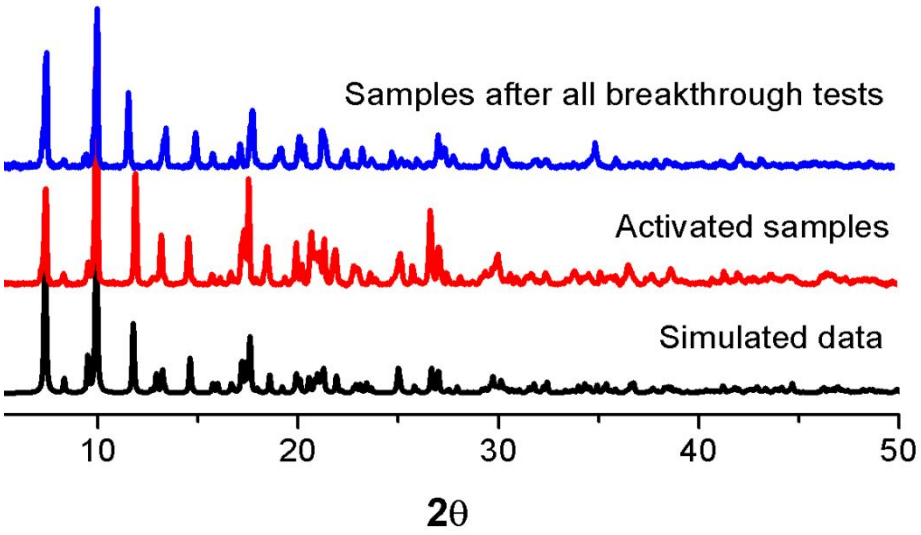

Figure S1. A comparison of PXRD patterns of the simulated data, the as-synthesized samples after 140°C activation, and the samples after all breakthrough experiments.

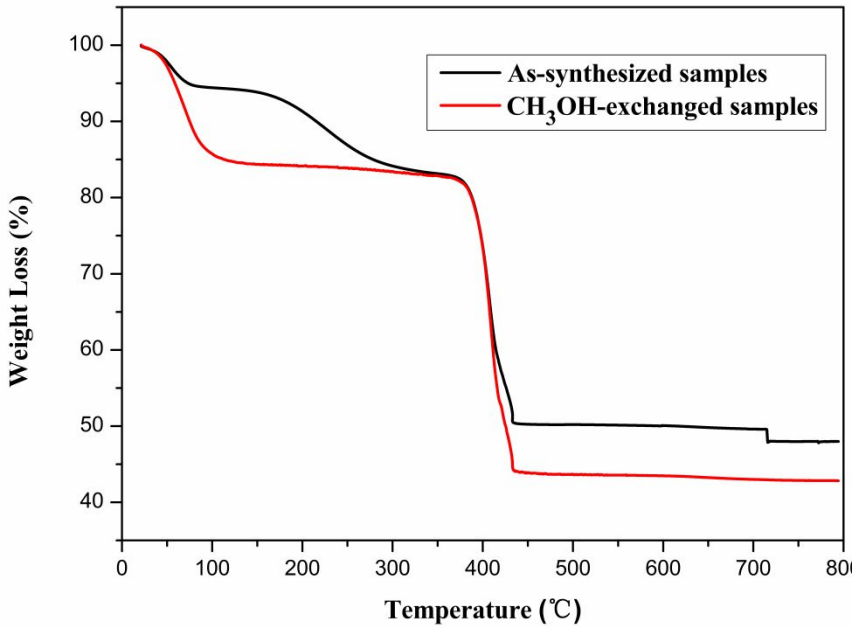

Figure S2. The TG polt of **ECUT-100** and the CH_3OH-exchanged Samples

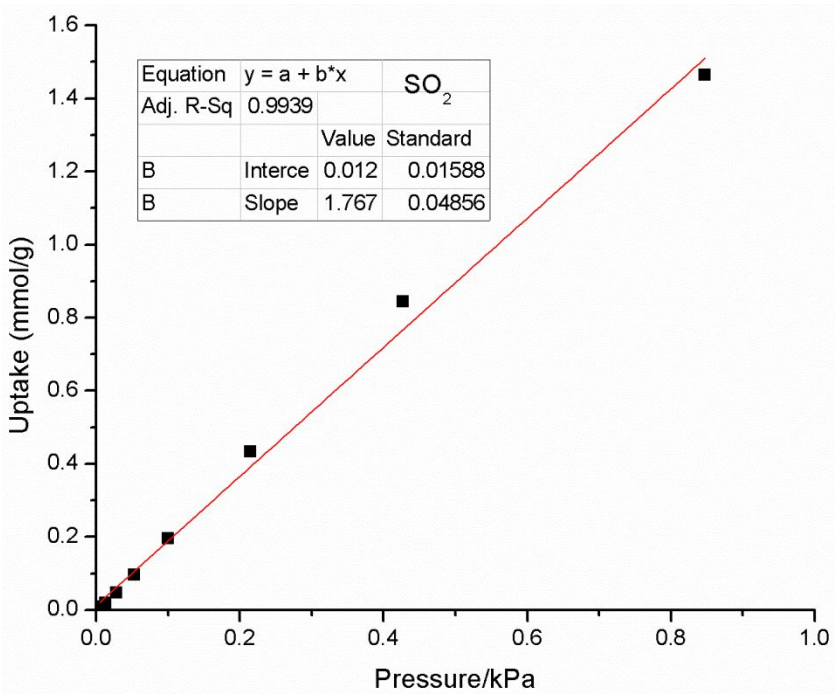

Figure S3. The Henry fitting of SO_2 adsorption on **ECUT-100**.

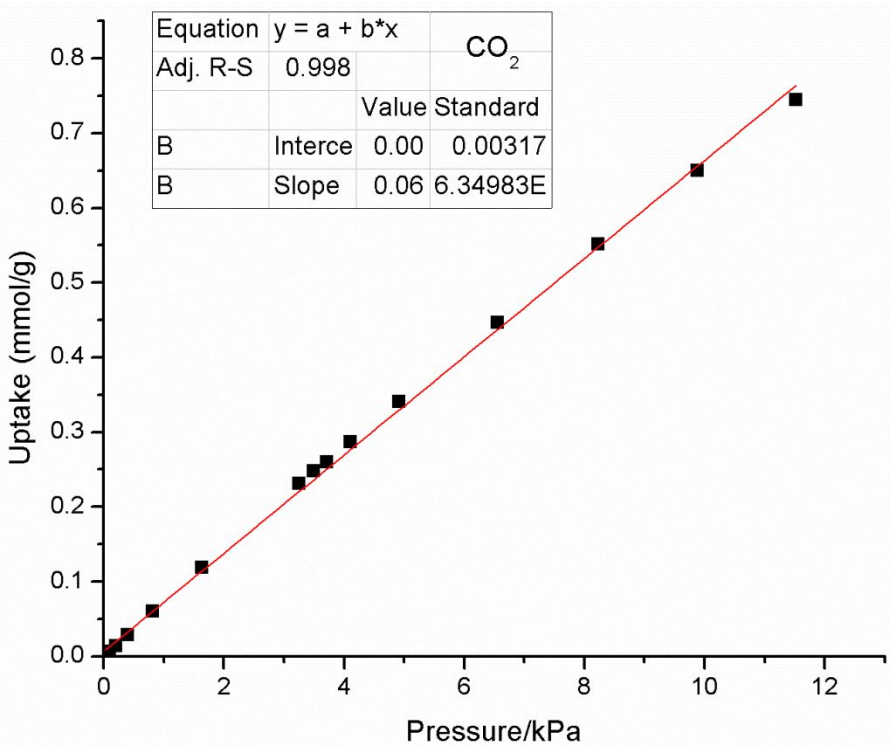

Figure S4. The Henry fitting of CO_2 adsorption on **ECUT-100**.

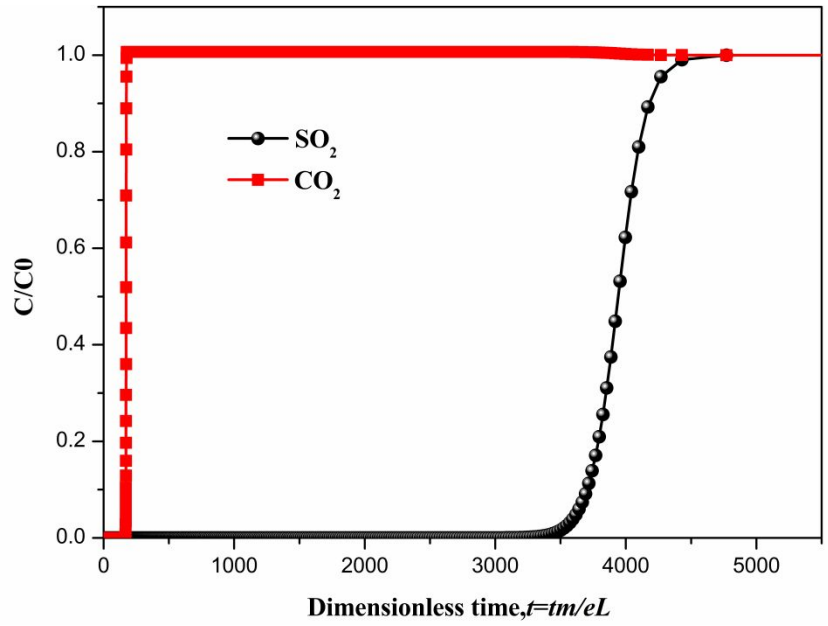

Figure S5. The transient breakthrough simulations for a 1:99 v/v SO_2/CO_2 mixture based on **ECUT-100** bed.

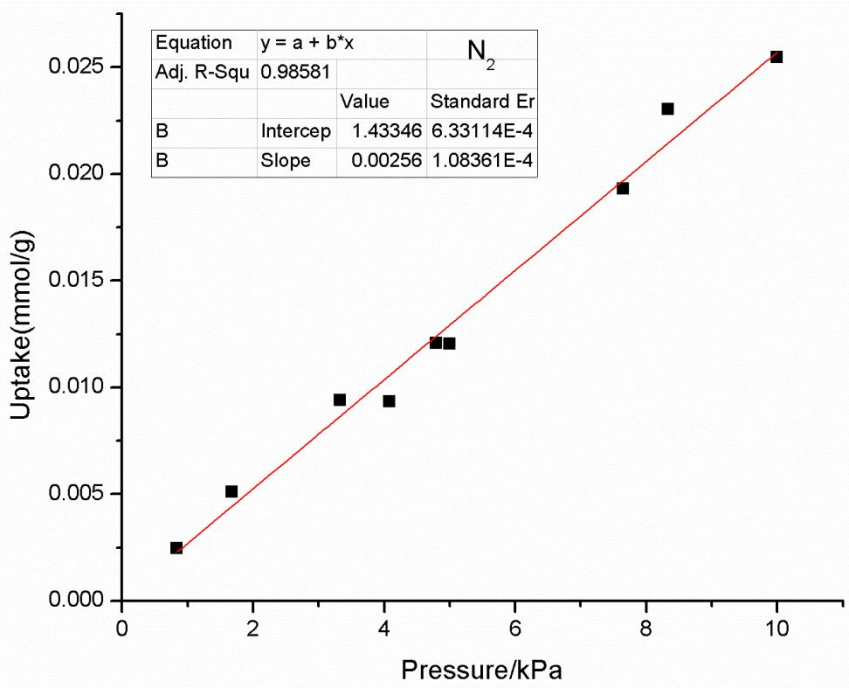

Figure S6. The Henry fitting of N_2 adsorption on **ECUT-100**.

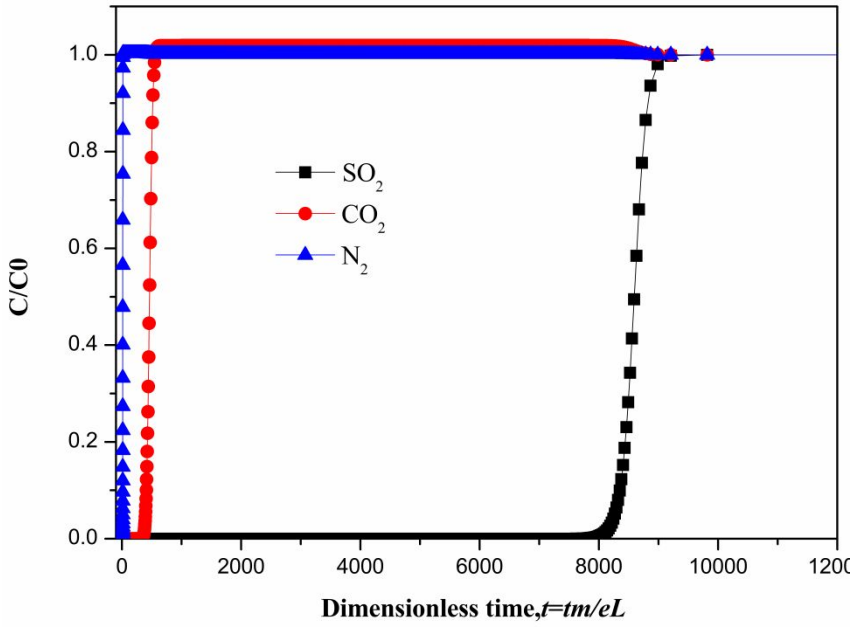

Figure S7. The transient breakthrough simulations for a 1:49.5:49.5 v/v $SO_2/CO_2/N_2$ mixture based on **ECUT-100** bed.

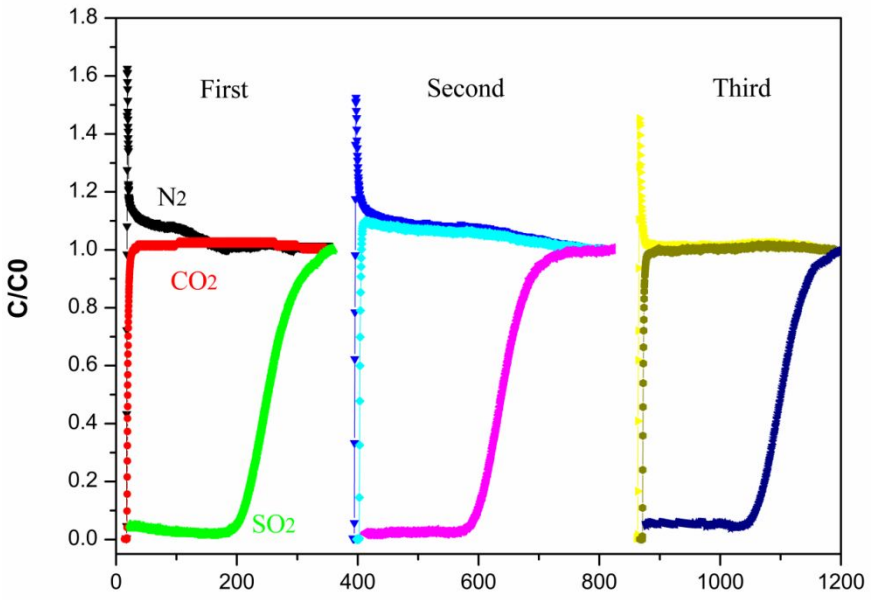

Figure S8. The recycle use of **ECUT-100** bed for separating $SO_2/CO_2/N_2$ mixture.

Figure S9. The photograph of **ECUT-100** and the samples after breakthrough tests.